Journal of Engineering for Gas Turbines and Power. Received July 27, 2018;
Accepted manuscript posted August 23, 2018. doi:10.1115/1.4041249

Gas Turbine Fouling: A comparison Among One Hundred Heavy-Duty Frames

Nicola Aldi[1], Nicola Casari[1], Mirko Morini[2], Michele Pinelli[1], Pier Ruggero Spina[1], Alessio Suman[1]

[1] Dipartimento di Ingegneria, Università degli Studi di Ferrara, 44122 Ferrara, Italy

[2] Dipartimento di Ingegneria e Architettura, Università degli Studi di Parma, 43121 Parma, Italy

ABSTRACT

Over recent decades, the variability and high costs of the traditional gas turbine fuels (e.g. natural gas), have pushed operators to consider low-grade fuels for running heavy-duty frames. Synfuels, obtained from coal, petroleum or biomass gasification, could represent valid alternatives in this sense. Although these alternatives match the reduction of costs and, in the case of biomass sources, would potentially provide a CO_2 emission benefit (reduction of the CO_2 capture and sequestration costs), these low-grade fuels have a higher content of contaminants. Synfuels are filtered before the combustor stage, but the contaminants are not removed completely. This fact leads to a considerable amount of deposition on the nozzle vanes due to the high temperature value. In addition to this, the continuous demand for increasing gas turbine efficiency, determines a higher combustor outlet temperature. Current advanced gas turbine engines operate at a turbine inlet temperature of (1400 – 1500) °C which is high enough to melt a high proportion of the contaminants introduced by low-grade fuels. Particle deposition can increase surface roughness, modify the airfoil shape and clog the coolant passages. At the same time, land based power units experience compressor fouling, due to the air contaminants able to pass through the filtration barriers. Hot sections and compressor fouling work together to determine performance degradation.

This paper proposes an analysis of the contaminant deposition on hot gas turbine sections based on machine nameplate data. Hot section and compressor fouling are estimated using a fouling susceptibility criterion. The combination of gas turbine net power, efficiency and turbine inlet temperature (TIT) with different types of synfuel contaminants highlights how each gas turbine is subjected to particle deposition. The simulation of particle deposition on one hundred (100) gas turbines ranging from 1.2 MW to 420 MW was conducted following the fouling susceptibility criterion. Using a simplified particle deposition calculation based on TIT and contaminant viscosity estimation, the analysis shows how the correlation between type of contaminant and gas turbine performance plays a key role.

The results allow the choice of the best heavy-duty frame as a function of the fuel. Low-efficiency frames (characterized by lower values of TIT) show the best compromise in order to reduce the effects of particle deposition in the presence of high-temperature melting

contaminants. A high-efficiency frame is suitable when the contaminants are characterized by a low-melting point thanks to their lower fuel consumption.

INTRODUCTION

Land-based gas turbines used in power plants or compressor stations experience performance losses which are due to the fouling of the compressor [1, 2] and, when gas turbines run with low-grade fuels, to the fouling of the turbine [3 – 6]. In most applications, low-grade fuels are coal, biomass and oil-residue petcoke. These fuels are gasified to produce syngas suitable for gas turbines operation. Syngas is usually contaminated by different levels of impurities depending on the type of source and filtration operations. Typically it contains traces of fly-ash particles having a diameter that ranges from 1 μm to 10 μm [7]. Matching a contaminant concertation of 1/10 parts per million by weight with high mass flow rate swallowed by a heavy-duty frame of hundreds of kilograms per second, the ingested materials could be equal to a few tons during a thousand operating hours [7]. These contaminants are heated up in the combustor determining deposition, erosion and corrosion on turbine components, especially on the first gas turbine stage. The result of particle impact on gas turbine hot sections depends in large part on the particle temperature that could be considered almost equal to the gas temperature.

Particle temperature determines the physical state of the impacting particle (solid, liquid or vapor), and in turn, determines the effects of particle impact (erosion or adhesion). Experimental analyses [4] and [8 – 10] and more recently accelerated particle deposition tests [11] have shown a dramatic variation of the effects of particle impact as a function of the gas temperature. Above a certain temperature, usually called the softening temperature [12], particles become sticky and their impacts on the gas turbine surface generate deposits. As reported in [12] at the softening temperature ash is making a transition from an initial deformation temperature to fluidity, assuming a plastic-like state with great capability to stick. Each low-grade fuel contaminant is characterized by a certain composition and due to this, each material has its temperature-dependent characteristics. Since first-stage turbine components operate at the highest temperatures, deposition usually takes place on the first-stage nozzle. Below this temperature, particle impact typically determines surface erosion [13].

In the light of this physical behavior of the contaminants introduced in the gas turbine hot section, the TIT assumes even greater importance, especially because TIT is directly correlated to the gas turbine efficiency. As reported in [14] and [15], gas turbine technology has evolved increasing the TIT up to 1500 °C determining a maximum efficiency of up to 40 % (considering for example the evolution from the E-type to H-type families of General Electric gas turbines [15]). Therefore, technological improvements have increased firing temperature values and efficiencies of gas turbines, but at the same time, have increased the problem related to semi-molten particle impact at the first turbine stage.

Aim of the paper. In this work, a comparison of one hundred (100) heavy-duty gas turbines considering the issues related to different contaminants due to the operation with low-grade fuels is proposed. The analysis is based on very different gas turbines considering net power, that ranges from 1.2 MW to 420 MW and efficiency, that ranges from 24 % to 40 %. In the present analysis, the issues of the hot section is very much a function of the fuel characteristics and quality.

The comparison, starting from the gas turbine nameplate data, is based on the consideration of the same amount of net energy provided by the gas turbine. Therefore, high-efficiency gas turbines consume a lower amount of fuel than low-efficiency frames for generating the same energy, but at the same time, high-efficiency gas turbines are characterized by higher TIT values and thus, more detrimental conditions related to particle sticking. The amount of contaminant (directly related to the mass of burned fuel) that affects the hot sections will be less or it may be stickier as a function of the TIT value.

Gas turbine selection is also proposed in relation to compressor fouling issues. The estimation of the power unit fouling sensitivity and susceptibility due to particle deposition on compressor sections is modeled using a literature index [14]. The technological era of the gas turbine has to be matched with the nature of the contaminants and characteristics related to gas turbine net power, efficiency and TIT value.

NOMENCLATURE

A	model coefficient
B	model coefficient
E	Energy
m	mass flow rate
n	number of oxygen atoms in the molecule
P	power
T	Temperature
W	Power

Greek letters

η	efficiency
Λ	optical basicity
μ	viscosity
ξ	ash content
χ	mole fraction

Subscripts and superscripts

air	air
C	corrected
c	critical
CM	Compressor
cont	contaminant
f	filtration
fuel	fuel
i	index
NC	non-corrected
net	net
soft	softening (referred to the particle behavior)
tot	total

Acronyms

ALS	Alstom
GE	General Electric
KHI	Kawasaki Heavy Industries
LHV	Low Heating Value
MAN	MAN Diesel & Turbo
MTSB HIT	Mitsubishi Hitachi
NPL	National Physical Laboratory
NWR	Net Working Ratio
PR	Pressure Ratio
RH	Relative Humidity
SIE	Siemens
SOL	Solar Turbines
SP	Sticking Probability
TIT	Turbine Inlet Temperature

Journal of Engineering for Gas Turbines and Power. Received July 27, 2018;
Accepted manuscript posted August 23, 2018. doi:10.1115/1.4041249

FLY-ASH CONTAMINANT CHARACTERISTICS AND STICKING MODEL

Low-grade fuels such as syngas could be obtained by from several raw materials such as coal, biomass or residual oil [16 – 19]. In this paper the selection of low-grade fuels was conducted considering these three different sources. In the following, composition and characteristics are listed as well as the model prediction for the particle viscosity and particle sticking probability.

Contaminants. This analysis is based on contaminants which are related to five (5) different low-grade fuels. Table 1 reports their chemical composition as a weight fraction of sodium oxide Na_2O, potassium oxide K_2O, calcium oxide CaO, magnesium oxide MgO, silicon dioxide SiO_2, aluminum trioxide Al_2O_3, titanium dioxide TiO_2 and iron trioxide Fe_2O_3. The chemical composition refers to the ash generated by the combustion of the related fuel. Obviously, these oxides do not cover the entire composition for each fuel but these individual oxides are thought to be the most important in characterizing their physical behavior. Minor elements are present in the chemical composition of fuel. According to the Phyllis 2 database [20] minor components (such as cobalt, cadmium, vanadium, etc.) were founded in several fuels especially biomass and coal but at the same time, do not greatly influence the physical characteristics of the fuels.

These silica melts are based on the strong covalent bond between silicon and oxygen forming a network structure. Different compositions lead to different softening temperatures which are related to particle deposition issues as reported in the next section. Each contaminant, associated with its correspondent low-grade fuel, is characterized by a specific softening temperature. Some of these contaminants (generated by the use of low-grade fuels such as petcoke, straw, coal and Pittsburgh) were used for studying particle deposition during experimental tests related to gas turbine hot section fouling. In particular, petcoke was used in [11] for studying particle deposition on coupon, straw in [7] and coal in [7], [11] and [21 – 24] were used for particle deposition on coupons, while Pittsburgh particle was used in [25]. The last contaminants named VAT-1 and VAT-2 are common coal-type particles and their characteristics are reported in [26].

Softening temperature values, that characterize the five (5) contaminant types used in this work, are taken from literature if available, or have been calculated by applying the model of Yin *et al.* [27]. This model allows the calculation of the softening temperature according to the chemical composition.

The ash content [%] reported in Table 1 was estimated using literature data, according to the reported notes (see Table 1 for reference). The ash content values were found in literature for the dry condition and refer to the part of the fuel that determines volatile matter during combustion. This matter does not contribute to combustion, but determines the subsequent contamination of the hot gas supplied by the burner to the gas turbine hot sections. Therefore, different fuels are characterized by a different ash content determining different hot section contamination (without considering the sticking capability of each type of fuel that depends on its chemical composition and

TIT value). In [26] a detailed explanation about the chemical composition analysis is reported. The ash content of each fuel is analyzed by X-ray fluorescence in order to extract the composition (in terms of oxides) of each ash.

Particle sticking model. The model adopted in this work for estimating particle adhesion is the critical viscosity model. This model, widely used in literature, compares actual particle viscosity to a reference viscosity at which sticking starts. In addition, the model could account for the stickiness of the deposit itself [28]. The sticking probability was assumed to be inversely proportional to viscosity. In terms of sticking probability, viscosity at or below the critical viscosity means the particle has a sticking probability (SP), whereas at other viscosity values (and thus, at lower temperatures) according to the relation

$$\mathrm{SP} = \mu_c/\mu \;\; ; \;\; \mu_c = \mu_{\mathrm{soft}} \tag{1}$$

where SP is the sticking probability and μ_{soft} is the particle viscosity at the softening temperature while μ is the viscosity of the particle at its actual temperature. Therefore

$$\mathrm{SP} = \begin{cases} \mu_c/\mu & \mu > \mu_c \\ 1 & \mu \leq \mu_c \end{cases} \tag{2}$$

Many authors have applied this method and, in some cases, validated its results with experimental tests [29 – 35].

Viscosity model. The aim of this study is to compare the operation of different gas turbines working with different low-grade fuels. Each gas turbine is characterized by its own TIT, that, together with contaminant composition, determines particle viscosity. The relation between fuel ash composition and melting point (and in turn, fuel ash viscosity) is very difficult to predict in detail [36]. The nature of the material structure (amorphous, crystalline, etc.) influences the temperature-dependent material characteristics.

For the aim of this study, it is possible to use as particle viscosity, the viscosity value provided by a simplified model. In this work, the particle viscosity is calculated according to the NPL (National Physical Laboratory) model reported in [37] with its corrections proposed in [38, 39], shown in detail in Appendix A. This model, as well as other viscosity models used for silica melt composites [40 – 43], only considers the major components of fuel ash such as those reported in Table 1.

THE SUSCEPTIBILITY OF THE HOT SECTION

Starting from the definition of the compressor's propensity to foul [14], this analysis refers to the susceptibility of gas turbines to particle deposition in the hot gas sections. The susceptibility is defined as the gas turbine propensity (in this case, the hot sections of the gas turbine) to fouling given certain operating conditions especially related to environment and fuel. It is important to note that susceptibility should not be confused with gas turbine fouling sensitivity that represents the impact of fouling on its performance.

In order to estimate the gas turbine fouling susceptibility related to particle deposition in hot sections, the following procedure is proposed. Each fuel is characterized by its ash content (see Table 1) that represents the amount of contaminant generated by its combustion. At the same time, filtration and separation systems are also adopted in order to reduce the amount of dangerous particles

Journal of Engineering for Gas Turbines and Power. Received July 27, 2018;
Accepted manuscript posted August 23, 2018. doi:10.1115/1.4041249

carried by the fuel from the gasifier to the gas turbine combustor. For these reasons, a general expression of an index able to represent the amount of contaminant m_{cont} that affects the gas turbine hot section can be defined as

$$m_{\text{cont}} = m_{\text{fuel}} \cdot (1 - \eta_{\text{f}}) \cdot \xi \cdot \text{SP} \tag{3}$$

where m_{fuel} is the mass flow rate of fuel, η_{f} is the filtration/separation efficiency, ξ is the ash content and SP is the sticking probability. Therefore, the value of m_{cont} reflects the actual mass of contaminant that affects the hot sections per unit of time. Regarding the filtration and separation systems, several different technologies exist that work according to different particle diameter ranges. Usually, these systems allow a dramatic reduction of the contaminant carried by the gas, even if the exact filtration efficiency depending on the contaminant size, and therefore proper characterization would be required [44]. This analysis aims to compare several different power units operating with different types of fuel and for this reason the filtration efficiency is not considered and the values of m_{cont} proposed in this paper, are representative of the fouling intensity that involves the gas turbine hot sections in qualitative way. The sticking probability value is calculated according to the particle viscosity, which is a function of TIT according to the aforementioned relations (see Eq. 1 and 2).

This analysis implies more detrimental conditions than the actual conditions in gas turbines. It is indeed well known that only a part of the incoming particles will actually impinge on and, eventually, stick to the inner surfaces of the hot section. A parameter that has been defined for quantifying such value is the capture efficiency, defined as the mass that sticks to a surface with respect to the total mass processed by the machine [30], [34]. Nonetheless, this value is generally unknown and its prediction is very challenging (experimental tests rather than computational studies are required). In light of these remarks, the capture efficiency has been considered to be the same for all the turbines investigated and its value is only related to the sticking probability of the case in question.

The amount of fuel can be calculated according to

$$m_{\text{fuel}} = \frac{E_{\text{tot}}}{\text{LHV}} \tag{4}$$

where the total energy E_{tot} represents the total energy consumed by the power unit for generating the target net energy E_{net}

$$E_{\text{tot}} = \frac{E_{\text{net}}}{\eta} \tag{5}$$

where η is the gas turbine efficiency. In this work a representative value of 25,000 kJ/kg of LHV was adopted for each low-grade fuel.

Through this procedure, it is possible to compare the amount of contaminant for different gas turbines (different values of efficiency and TIT) and fuels (different ash contents coupled with different SP values).

COMPARATIVE ANALYSIS

In this section the comparison of one hundred (100) gas turbines is proposed including older technology units as well as advanced models with a wide span of characteristics. The present engine selection is based on the engine characteristics. Some power units operate typically with gaseous fuels rather than liquid fuels and vice versa. In this work, the correlation between fuel quality and hot section fouling is carried out considering the engine characteristics beyond the actual application.

To improve the quality and the completeness of this comparison, an index related to compressor fouling is also considered. With the reference of Meher-Homji *et al.* [14], the effects of fouling in the compressor section on power unit performance is well represented by the Net Working Ratio (NWR). This index is a good predictor of both gas turbine susceptibility and sensitivity to compressor fouling. The NWR is defined as follows

$$\mathrm{NWR} = \frac{W_{\mathrm{TB}} - W_{\mathrm{CM}}}{W_{\mathrm{TB}}} = 1 - \frac{W_{\mathrm{CM}}}{W_{\mathrm{TB}}} \tag{6}$$

where W_{CM} is the compressor power while W_{TB} is the gas turbine power. Thus, NWR requires an estimation of the turbine section work and compressor consumption which are usually not provided by the manufacturer. The NWR index is only representative of the compressor fouling effects on gas turbine performance and does not account for the effects of turbine fouling. For this reason, in this paper m_{cont} values (representative of turbine fouling) and NWR values (representative of compressor fouling) which characterize each gas turbine operating with a specific low-grade fuel are considered for power unit comparison.

Turbine data. This analysis is based on the GTPRO® v.24.0 by Thermoflow Inc. database and the data are based on GTPRO® estimates and calculations. For each gas turbine, the TIT and NWR values were calculated according to the following operating conditions. Each gas turbine runs at 100 % rating with inferred TIT control mode and is fueled by natural gas supplied at 25 °C at the minimum allowable pressure depending on the gas turbine. Reasonable inlet and outlet pressure losses were set equal to about 980 Pa and 1230 Pa, respectively. Each simulation was performed assuming 101,325 Pa, 15 °C and 60 % RH as ambient conditions.

For clarification purposes, all data are reported in Appendix B, while in this section only an overall comparison is provided. Figure 1 shows the relation between net power, efficiency, TIT and NWR values. The data are grouped according to the power, less than 10 MW, higher than 10 MW and less than 100 MW, and finally higher than 100 MW, by means of three indicator shapes: bullets, squares and diamonds, respectively. The intention of these figures is to indicate the general relationship between the most important nameplate characteristics of several different power units.

Figure 1a shows the relation between gas turbine net power and efficiency: as the gas turbine size increases, the efficiency increases as well. The data are comprised in quite a narrow band. It can be noted that this selection comprises gas turbines with very low efficiency (about 24 %) and high-efficiency frames (the peak of efficiency is equal to 40 %) over a net power variation of two orders of magnitude.

Based on this net power range, Figure 1b proposes the relation with the TIT values. In this case the relation appears weaker than the previous one. As reported in [14, 15], comparing a number of gas turbines designed over decades, it is possible to highlight different technological aspects. For example, older heavy duty gas turbine designs tend to have low turbine inlet temperatures and low cycle pressure ratios (up to 10), while modern gas turbines have modest pressure ratios (up to 16) but operate at higher TIT. By increasing the TIT value, the efficiency of the gas turbine increases. As can be seen from Figure 1c, the relation between TIT and gas turbine efficiency is clearly visible. The data belong to a narrow band showing the strong relation between TIT and efficiency. Based on the analysis reported in [14], the specific work of the gas turbine increases according to the pressure ratio and the TIT values but at the same time, gas turbine efficiency increases according to the TIT. Similar considerations can be made for the NWR values reported in Figure 1d where the correlation between efficiency and NWR confirms the evaluations reported in [14]: high efficiency values are related with high values of TIT and NWR.

Considering these relations, the importance of considering the contaminant characteristics (especially those related to sticking capability), due to operation with low-grade fuels, during the turbine selection and for the best power plant management, is clearly visible.

Comparison. With the reference of gas turbine nameplate data, Figure 2 reports the net power and efficiency values for the considered gas turbines. The bar charts report the data in alphabetical order, without considering the gas turbine characteristics. The data are grouped as in Figure 1, by means of a gray scale reported above the bar charts. Starting from these data, including the value of TIT, it is possible to calculate the total amount of contaminant that sticks to the gas turbine hot sections according to the previous procedure. Considering 1 GWh of net energy and the gas turbine efficiency, the total amount of fuel can be calculated. Therefore, considering the TIT value and the ash content, the particle sticking probability is evaluated and a value representative of the total amount of contaminant able to stick to the walls is calculated according to Eq. (3). The sticking probability depends on the TIT and on the softening temperature of the contaminant reported in Table 1.

Figure 3 reports the NWR values and the amount of contaminant that sticks to the hot section for the investigated gas turbines. The data are ordered by gas turbine efficiency from lower to higher values and divided according to the five different contaminant types. Also in this case, the data are grouped by three power ranges, according to the gray scale reported above the graphs. Given the definition proposed in Eq. (3), the lower m_{cont} the lower the fouling rate. Considering the contaminant generated by petcoke ash, the trend according to the different gas turbines is opposite to the efficiency. This is directly related to the TIT values. The softening temperature of petcoke is lower than all TIT values considered in this analysis and it sets SP equal to 1 for all power units. For this reason, high-efficiency turbines are characterized by lower values of m_{cont} and are thus the optimal choice for that contaminant.

Moving on to the other contaminants, characterized by higher softening temperatures, the scenario changes. Gas turbines characterized by lower efficiencies tend to be more interesting since they are characterized by lower values of m_{cont} than the high-efficiency units. In fact, the worst scenario for high-efficiency units is represented by the VAT-1 (see Figure 3f) contaminant-type. This contaminant has the highest softening temperature value, determining high values of SP for high-efficiency gas turbines. As reported in Figure 1c higher efficiency values are associated with higher TIT values.

The last consideration is related to the correlation between gas turbine efficiency and the amount of contaminant. Considering for example the results obtained for VAT-2 and Pittsburgh–type ash contaminant, trends are characterized by sharp slope variations. This means that by changing the target efficiency by even a small percentage during the turbine selection, the contamination of the hot section changes dramatically.

Figure 4 reports the amount of contaminant that sticks to the hot section ordered by gas turbine net power. Gray scale indicates the power ranges as reported in the previous analysis. For the sake of brevity, only two contaminants are reported, straw and Pittsburgh, characterized by two different softening temperature values, 1213 K and 1589 K respectively. The overall trends are similar to the previous ones even if, for the middle-rate gas turbine, the data comprised in the range of (10 – 100) MW appear more dispersed. Based on the power plant requirements, operators can select more appropriate configurations of the power units. As a function of the low-grade fuel type, it is possible to find the configuration of two or three units in substitution of a single unit (if possible) in order to limit the gas turbine fouling. As can be seen from Figure 4, low-rated power gas turbines are characterized by lower values of sticky contaminant compared to the high-rated power gas turbines.

Considerations. The comparisons proposed in Figure 3 and Figure 4 are based on the two most important parameters for a gas turbine: net power and efficiency. These two quantities are taken into account by the operators and plant designers for the selection of the appropriate power unit. The TIT value, that represents another indicator of the gas turbine performance, is not usually considered during selection even if it could be related to gas turbine performance degradation. With reference to the contaminant selection, it is possible to identify the best and worst performing gas turbine. Table 2 reports the ranking based on the amount of contaminant. Different gas turbines from different manufacturers are reported. With the contaminants characterized by the lowest TIT values, the worst performing gas turbines are those characterized by lower efficiency values. By contrast, for the contaminants with high softening temperature values, the most suitable gas turbines are those characterized by the best compromise between TIT value and efficiency.

This evaluation is related only to the fouling of the gas turbine hot sections but, in the real world, the compressor section is also subject to fouling issues. Power unit installation as well as the environmental contaminant and the performance of the filtration system determine compressor fouling [1].

In the last part of this work, the results can be related to the analysis reported in [14] regarding power unit susceptibility and sensitivity to compressor fouling. As mentioned in the previous section, by means of NWR, it is possible to estimate the gas turbine susceptibility and sensitivity to compressor fouling. Lower NWR values represent the engines where a higher portion of the total turbine work is consumed in the compressor. These engines tend to be more susceptible and sensitive to compressor fouling. Therefore, by matching these results with the susceptibility of the hot sections (represented by m_{cont} values) it is possible to determine which gas turbine represents the best compromise as a function of the ash contaminant type. In Figure 3 and Figure 4 the NWR value for each gas turbine is depicted as a bar chart. According to the efficiency values, the NWR does not follow a monotonic trend and some peculiarities exist in particular for lower and higher efficiency values. In fact, power units named GE PGT2, ALS GT5 and SOL Titan 250 show significant lower values of NWR than similar power units (in terms of efficiency). On the other hand, taking into consideration the order proposed in Figure 4, for similar power, different gas turbines show differences in NWR values up to 0.07. Given this, Figure 5 reports a comparison between different gas turbines grouped by similar power 10±1 MW, 50±5 MW and 100±10 MW. For a given power, the data are ordered by gas turbine NWR from lower to higher values for the five ash contaminant types.

Differences related to the ash content and to the softening temperature which distinguish each contaminant characterize the comparison proposed in Figure 5.

Each power unit experiences performance drops due to the fouling of compressor and turbine sections estimated by NWR and m_{cont}, respectively. According to their definition, the two indexes used in this comparison are not directly correlated. In particular, the NWR value, that represents the compressor fouling index, is a consequence of the power unit design, operating conditions (such as pressure, temperature and humidity) and load. The m_{cont} value, that represents the turbine fouling index, is a consequence of the TIT value, the ash content of the fuel and the sticking probability of contaminant particles. An embryo relationship can be explained by considering the correlation between TIT and NRW values. Figure 6 reports the data dispersion that appears very similar to those reported in Figure 1d (NWR values vs. gas turbine efficiency). Lower NWR values and thus, higher gas turbine susceptibility to compressor fouling, correspond to lower TIT values that imply lower efficiency values. These units are suitable for operating with contaminants characterized by higher softening temperature. By contrast, higher NWR values (lower gas turbine susceptibility to compressor fouling) correspond to higher values of TIT and efficiency. These units are suitable for operating with contaminants characterized by lower softening temperature.

As reported in Figure 5, operators are required to carefully evaluate the combination of the effects of compressor fouling and hot section fouling during the design of each installation. They have to consider the location, the environment and the operating conditions

for estimating the impact of compressor fouling on the unit performance [1], but they also have to take into account the effects of the low-grade fuel in relation to net power, efficiency and reliability requirements.

In Figure 7 the global overview of the relationship between gas turbine efficiency, NWR and m_{cont} is proposed. In addition, the power units analyzed in Figure 5 are addressed. The data are grouped by three power ranges, lower than 10 MW, higher than 10 MW and lower than 100 MW, and finally higher than 100 MW, by means of three indicator shapes: bullets, squares and diamonds, respectively. Taking into consideration the amount of contaminant and NWR and efficiency values, the selection of the appropriate gas turbine is not straightforward.

Requirements of high efficiency power units collide with the susceptibility and sensitivity to turbine fouling. High-efficiency frames are characterized by higher values of NWR but, in the case of higher-melting contaminants (higher softening temperatures, such as Pittsburgh and VAT-1 ash contaminants) are the worst solution in terms of fouling issues.

In light of these results, the use of cycle simulation tools assisted by these considerations could represent a valid support for both manufacturers and operators. Therefore, the power plant design could be driven by fouling reduction as a new paradigm.

Limitations. The results proposed in this paper have been affected by some limitations. The values of NWR and TIT used for calculating the gas turbine sensitivity and susceptibility to compressor and turbine fouling refer to ISO operating conditions. However, gas turbines which operate at different ambient conditions and/or with different loads could experience different NWR values and the gas turbine inlet temperature could be slightly different. By referring the analysis to ISO conditions which represent an international standard, the results are suitable for comparing several different power units relating to different design requirements and specifications.

The definition of the hot section susceptibility reported in this paper is based on a black box-type analysis where the evaluation of the sticking probability is based only on the TIT values and not on actual behavior (temperature, velocity, size, etc.) of the contaminants. Similar considerations can be done for the compressor sections. Particles stick on the blade surface depending on the several parameters (e.g. dimension, impact velocity, etc.) [45 – 47] and affect the blade surface in different ways [48, 49].

At the same time, hot section fouling is proposed without considering the actual employment of the selects gas turbines. Some of selected engines work with gaseous fuels and vice versa, other units operates with liquid fuels. This hypothesis allows the qualitative evaluation of the gas turbine propensity to foul using only the nameplate data and it is most affected by the fuel characteristics and quality. The sticking capability is calculated according to the critical viscosity method that is not an unambiguous method but is well known in literature and, as reported in this work, it is often used in numerical simulations.

In the future, the concept of gas turbine hot sections fouling susceptibility may be introduced and defined according to different particle sticking models, taking into consideration data availability and different compositions of the contaminants, as well as the hot section sensitivity to foul and erosion.

CONCLUSIONS

This paper addresses the susceptibility of the gas turbine hot section to fouling. Based on the definition of the contaminant involved in the low-grade fuel used for heavy-duty applications, the hot section susceptibility was defined according to the gas turbine nameplate data. Gas turbine efficiency and net power values are used for comparing one hundred (100) heavy-duty frames.

The direct relation between the efficiency and the turbine inlet temperature implies the correlation between the type of contaminant and gas turbine fouling issues. For contaminants characterized by lower values of softening temperature, high-efficiency turbines are characterized by lower values of sticky contaminant representing the best choice for operators. Moving on to higher softening temperatures, low-efficiency gas turbines become the best choice. In fact, these units are characterized by lower values of turbine inlet temperature determining lower values of sticking probability. The classification of the power unit according to efficiency, net power and amount of sticky contaminant was proposed showing how slight variations of gas turbine characteristics determine huge variations in terms of sticky contaminant.

In addition to hot section deposition, heavy-duty gas turbines are affected by compressor fouling. From such a standpoint, the susceptibility and sensitivity of the compressor to fouling were matched with the hot section susceptibility. This extensive analysis has shown that the combination of compressor and hot section fouling is not univocal and has to be carefully evaluated by manufacturers and operators.

Gas turbine susceptibility and sensitivity are then related to both compressor and the turbine. Each manufacturer and operator has to consider the location, the environment and the effects of low-grade fuel in order to obtain the best performance for each installation according to different criteria, such as, installed power, fuel-saving, reliability and operability.

ACKNOLEDGMENTS

The Authors wish to thank Dr. Elettra Fabbri for her valuable support for calculating contaminant characteristics and properties.

REFERENCES

[1] Suman A., Morini M., Aldi N., Casari N., Pinelli M., Spina P.R. A compressor fouling review based on an historical survey of asme turbo expo papers (2017) Journal of Turbomachinery, 139 (4), art. no. 041005. DOI: 10.1115/1.4035070.

[2] Kurz R., Brun K. Fouling mechanisms in axial compressors (2012) Journal of Engineering for Gas Turbines and Power, 134 (3), art. no. 032401. DOI: 10.1115/1.4004403.

[3] Schnittger J.R. The New 40-MW Gas Turbine of the Vastervik Central Station. (1962) American Society of Mechanical Engineers (Paper), 19 p. DOI: 10.1115/62-GTP-1

[4] Whitlow G.A., Lee S.Y., Mulik P.R., Wenglarz R.A., Sherlock T.P., Cohn A. A. Combustion turbine deposition observations from residual and simulated residual oil studies (1983) Journal of Engineering for Gas Turbines and Power, 105 (1), pp. 88–96. DOI: 10.1115/1.3227403.

[5] Wenglarz R.A., Cohn A. Turbine deposition evaluations using simplified tests (1983) American Society of Mechanical Engineers (Paper), 7 p. DOI: 10.1115/83-GT-115.

[6] Wenglarz, R.A. 1985. Deposition, erosion and corrosion protection for Coal-Fired gas turbines (1985) Proceedings of the ASME Turbo Expo, 2. DOI: 10.1115/85IGT61.

[7] Bons J.P., Crosby J., Wammack J.E., Bentley B.I., Fletcher T.H. High-pressure turbine deposition in land-based gas turbines from various synfuels (2007) Journal of Engineering for Gas Turbines and Power, 129 (1), pp. 135–143. DOI: 10.1115/1.2181181.

[8] Bowden A.T., Draper P., Rowling H. The Problem of Fuel-oil Ash Deposition in Open-cycle Gas Turbines (1953) Proceedings of the Institution of Mechanical Engineers, 167(1), pp. 291–312. DOI: 10.1243/PIME_PROC_1953_167_035_02

[9] Wenglarz R.A., Fox Jr R.G. Chemical aspects of deposition/corrosion from coal-water fuels under gas turbine conditions (1990a) Journal of Engineering for Gas Turbines and Power, 112 (1), pp. 1–8. DOI: 10.1115/1.2906471.

[10] Wenglarz R.A., Fox Jr R.G. Physical aspects of deposition from coal-water fuels under gas turbine conditions (1990b) Journal of Engineering for Gas Turbines and Power, 112 (1), pp. 9–14. DOI: 10.1115/1.2906484.

[11] Crosby J.M., Lewis S., Bons J.P., Ai W., Fletcher T.H. Effects of Temperature and Particle Size on Deposition in Land Based Turbines (2008) Journal of Engineering for Gas Turbines and Power;130 (5), art. no. 051503. DOI: 10.1115/1.2903901.

[12] Sreedharan S.S., Tafti D.K. Composition dependent model for the prediction of syngas ash deposition with application to a leading edge turbine vane (2010) Proceedings of the ASME Turbo Expo, 4 (Parts A and B), pp. 615–626. DOI: 10.1115/GT2010-23655.

[13] Tabakoff W. Review-turbomachinery performance deterioration exposed to solid particulates environment (1984) Journal of Fluids Engineering, Transactions of the ASME, 106 (2), pp. 125–134. DOI: 10.1115/1.3243088.

[14] Meher-Homji C.B., Chaker M., Bromley A.F. The fouling of axial flow compressors - Causes, effects, susceptibility and sensitivity (2009) Proceedings of the ASME Turbo Expo, 4, pp. 571–590. DOI: 10.1115/GT2009-59239.

[15] Unger D., Herzog H. Comparative Study on Energy R&D Performance: Gas Turbine Case Study. Central Research Institute of Electric Power Industry (CRIEPI), 1998 - Technical Report.

[16] Morini M., Venturini M. An innovative inlet air cooling system for IGCC power augmentation - Part I: Analysis of IGCC plant components (2012) Proceedings of the ASME Turbo Expo, 3, pp. 859–869. DOI: 10.1115/GT2012-68346.

[17] Morini M., Pinelli M., Spina P.R. An innovative inlet air cooling system for igcc power augmentation - Part II: Thermodynamic analysis (2012) Proceedings of the ASME Turbo Expo, 3, pp. 871–881. DOI: 10.1115/GT2012-68352.

[18] Morini M., Pinelli M., Spina P.R., Vaccari A. An innovative inlet air cooling system for igcc power augmentation - Part III: Computational fluid dynamic analysis of syngas combustion in nitrogen-enriched air (2013) Proceedings of the ASME Turbo Expo, 2. DOI: 10.1115/GT2013-94094.

[19] Morini M., Pinelli M., Spina P.R., Vaccari A., Venturini M. Feasibility analysis of gas turbine inlet air cooling by means of liquid nitrogen evaporation for IGCC power augmentation (2015) Applied Thermal Engineering, 80, pp. 168–177. DOI: 10.1016/j.applthermaleng.2015.01.025.

[20] Phyllis2, database for biomass and waste, https://www.ecn.nl/phyllis2 - Energy research Centre of the Netherlands.

[21] Ai W., Laycock R.G., Rappleye D.S., Fletcher T.H, Bons J.P. Effect of particle size and trench configuration on deposition from fine coal flyash near film cooling holes (2011) Energy and Fuels, 25 (3), pp. 1066–1076. DOI: 10.1021/ef101375g.

[22] Ai W., Murray N., Fletcher T.H., Harding S., Lewis S., Bons J.P. Deposition near film cooling holes on a high pressure turbine vane (2012) Journal of Turbomachinery, 134 (4), art. no. 041013. DOI: 10.1115/1.4003672.

[23] Ai W., Murray N., Fletcher T.H., Harding S., Bons J.P. Effect of hole spacing on deposition of fine coal flyash near film cooling holes (2012) Journal of Turbomachinery, 134 (4), art. no. 041021. DOI: 10.1115/1.4003717.

[24] Laycock R.G., Fletcher T.H. Time-Dependent Deposition Characteristics of Fine Coal Fly Ash in a Laboratory Gas Turbine Environment. (2013) Journal of Turbomachinery, 135 (2), art. no. 021003. DOI: 10.1115/1.4006639.

[25] Anderson R.J., Romanowsky C.J., France J.E. The Adherence of Ash Particles from the Combustion of Micronized Coal. Morgantown Energy Technology Center, Res. Rep. DOE/METC-85/2007 (DE85008600); October, 1984.

[26] Trent V.A., Medlin J.H., Coleman S.L., Stanton R.W. Chemical Analyses and Physical Properties of 12 Coal Samples from the Pocahontas Field, Tazewell County, Virginia, and McDowell County, West Virginia. 1982. Geological Survey Bulletin 1528, United States Government Printing Office, Washington, US.

[27] Yin C., Luo Z., Ni M., Cen K. Predicting coal ash fusion temperature with a back-propagation neural network model (1998) Fuel, 77, pp. 1777–1782.

[28] Walsh P.M., Sayre A.N., Loehden D.O., Monroe L.S., Beér J.M., Sarofim A.F. Deposition of bituminous coal ash on an isolated heat exchanger tube: Effects of coal properties on deposit growth (1990) Progress in Energy and Combustion Science, 16 (4), pp. 327–345. DOI: 10.1016/0360-1285(90)90042-2.

[29] Sreedharan S.S., Tafti D.K. Composition dependent model for the prediction of syngas ash deposition with application to a leading edge turbine vane (2010) Proceedings of the ASME Turbo Expo, 4 (Parts A and B), pp. 615–626. DOI: 10.1115/GT2010-23655.

[30] Barker B., Casady P., Shankara P., Ameri A., Bons J.P. Coal Ash Deposition on Nozzle Guide Vanes-Part II: Computational Modeling (2012) Journal of Turbomachinery, 135 (1), art. no. 011014. DOI: 10.1115/1.4006399.

[31] Birello F., Borello D., Venturini P., Rispoli F. Modelling of deposit mechanisms around the stator of a gas turbine (2013) Proceedings of the ASME Turbo Expo, 2. DOI: 10.1115/GT2013-95688.

[32] Borello D., D'Angeli L., Salvagni A., Venturini P., Rispoli F. Study of particles deposition in gas turbine blades in presence of film cooling (2014) Proceedings of the ASME Turbo Expo, 5B. DOI: 10.1115/GT2014-26250.

[33] Prenter R., Whitaker S.M., Ameri A., Bons J.P. The effects of slot film cooling on deposition on a nozzle guide vane (2014) Proceedings of the ASME Turbo Expo, 3A. DOI: 10.1115/GT2014-27171.

[34] Zagnoli D., Prenter R., Ameri A., Bons .JP. Numerical study of deposition in a full turbine stage using steady and unsteady methods (2015) Proceedings of the ASME Turbo Expo, 2C. DOI: 10.1115/GT2015-43613.

[35] Dowd C., Tafti D., Kuahai Y. Sand transport and deposition in rotating two-passed ribbed duct with coriolis and centrifugal buoyancy forces at RE=100,000 (2017) Proceedings of the ASME Turbo Expo, 2D-2017. DOI: 10.1115/GT2017-63167.

[36] Taltavull C., Dean J., Clyne T.W. Adhesion of volcanic ash particles under controlled conditions and implications for their deposition in gas turbines (2016) Advanced Engineering Materials, 18 (5), pp. 803–813. DOI: 10.1002/adem.201500371.

[37] Mills K.C., Sridhar S. Viscosities of ironmaking and steelmaking slags (1999) Ironmaking and Steelmaking, 26 (4), pp. 262–268. DOI: 10.1179/030192399677121.

[38] Duffy J.A., Ingram M.D. Optical basicity—IV: Influence of electronegativity on the Lewis basicity and solvent properties of molten oxyanion salts and glasses (1975) Journal of Inorganic and Nuclear Chemistry, 37 (5), pp. 1203–1206. DOI: 10.1016/0022-1902(75)80469-6.

[39] Zhang G.H., Chou K.C. Simple method for estimating the electrical conductivity of oxide melts with optical basicity (2010) Metallurgical and Materials Transactions B: Process Metallurgy and Materials Processing Science, 41 (1), pp. 131–136. DOI: 10.1007/s11663-009-9298-z.

[40] Hoy H.R., Roberts A.G., Wilkins D.M. Behavior of Mineral Matter in Slagging Gasification Process (1965) I.G.E. Journal, pp. 444−69.

[41] Urbain G., Cambier F., Deletter M., Anseau M.R. Viscosity of Silicate Melts (1981) Transaction and journal of the British Ceramic Society, 80, pp. 139–141.

[42] Senior C.L., Srinivasachar S. Viscosity of Ash Particles in Combustion Systems for the Prediction of Particle Sticking (1995) Energy Fuels, 9, pp. 277–283.

[43] Giordano D., Russell J.K., Dingwell D.B. Viscosity of magmatic liquids: A model (2008) Earth and Planetary Science Letters, 271 (1-4), pp. 123-134. DOI: 10.1016/j.epsl.2008.03.038.

[44] Newby, R.A., Bannister, R.L., Miao, F. Westinghouse combustion turbine performance in coal gasification combined cycles (1996) ASME 1996 International Gas Turbine and Aeroengine Congress and Exhibition, GT 1996, 3. DOI: 10.1115/96-GT-231

[45] Suman, A., Kurz, R., Aldi, N., Morini, M., Brun, K., Pinelli, M., Spina, P.R. Quantitative computational fluid dynamics analyses of particle deposition on a transonic axial compressor blade-part I: Particle zones impact (2014) Journal of Turbomachinery, 137 (2), art. no. 021009. DOI: 10.1115/1.4028295

[46] Suman, A., Morini, M., Kurz, R., Aldi, N., Brun, K., Pinelli, M., Spina, P.R. Quantitative computational fluid dynamic analyses of particle deposition on a transonic axial compressor blade-part ii: Impact kinematics and particle sticking analysis (2015) Journal of Turbomachinery, 137 (2), art. no. 021010. DOI: 10.1115/1.4028296

[47] Suman, A., Kurz, R., Aldi, N., Morini, M., Brun, K., Pinelli, M., Ruggero Spina, P. Quantitative Computational Fluid Dynamics Analyses of Particle Deposition on a Subsonic Axial Compressor Blade (2016) Journal of Engineering for Gas Turbines and Power, 138 (1), art. no. 012603. DOI: 10.1115/1.4031205

[48] Suman, A., Morini, M., Kurz, R., Aldi, N., Brun, K., Pinelli, M., Ruggero Spina, P. Estimation of the Particle Deposition on a Transonic Axial Compressor Blade (2016) Journal of Engineering for Gas Turbines and Power, 138 (1), art. no. 012604. DOI: 10.1115/1.4031206

[49] Suman, A., Morini, M., Kurz, R., Aldi, N., Brun, K., Pinelli, M., Spina, P.R. Estimation of the particle deposition on a subsonic axial compressor blade (2017) Journal of Engineering for Gas Turbines and Power, 139 (1), art. no. 012604. DOI: 10.1115/1.4034209

APPENDIX A

The NPL method (National Physical Laboratory) [37] is able to predict the particle viscosity based on the composition and temperature according to the following procedure. This method is based on the optical basicity and the viscosity can be calculated according to

$$\ln \mu = \ln A_{\mathrm{NPL}} + \frac{B_{\mathrm{NPL}}}{T} \tag{A1}$$

where the temperature is expressed in [K] and the particle viscosity in [Pa s]. This model is generally applicable and not limited to slag of a certain composition. The model is based on the calculation of the optical basicity (that could be corrected for the cations required for the charge balance of the aluminum oxide) according to the mole fraction χ and number of oxygen atoms n in the molecule. The optical basicity is used to classify oxides on a scale of acidity, which is referred to the same O^{2-} base. Optical basicity of glasses and slags is derived from the Lewis acidity/basicity concept. The expression of the Non-Corrected (NC) optical basicity Λ^{NC} is the following

$$\Lambda^{\mathrm{NC}} = \frac{\sum \chi_{\mathrm{i}} n_{\mathrm{i}} \Lambda_{\mathrm{i}}}{\sum \chi_{\mathrm{i}} n_{\mathrm{i}}} \tag{A2}$$

where the values of the theoretical optical basicity Λ are listed in Table A1.

According to the correction proposed by Duffy and Ingram [38], used in [39], the Corrected (C) optical basicity Λ^{C} is calculated as

$$\chi_{\mathrm{CaO}} \geq \chi_{\mathrm{Al_2O_3}}$$

$$\begin{aligned}\Lambda^{\mathrm{C}} = (&1\,\Lambda_{\mathrm{CaO}}\left(\chi_{\mathrm{CaO}} - \chi_{\mathrm{Al_2O_3}}\right) + 2\,\Lambda_{\mathrm{SiO_2}}\,\chi_{\mathrm{SiO_2}} + 3\,\Lambda_{\mathrm{Al_2O_3}}\,\chi_{\mathrm{Al_2O_3}} + 1\,\Lambda_{\mathrm{MgO}}\,\chi_{\mathrm{MgO}} + 3\,\Lambda_{\mathrm{Fe_2O_3}}\,\chi_{\mathrm{Fe_2O_3}} + 1\,\Lambda_{\mathrm{Na_2O}}\,\chi_{\mathrm{Na_2O}} \\ &+1\,\Lambda_{\mathrm{K_2O}}\,\chi_{\mathrm{K_2O}} + 2\,\Lambda_{\mathrm{TiO_2}}\,\chi_{\mathrm{TiO_2}})/(1\left(\chi_{\mathrm{CaO}} - \chi_{\mathrm{Al_2O_3}}\right) + 2\,\chi_{\mathrm{SiO_2}} + 3\,\chi_{\mathrm{Al_2O_3}} + 1\,\chi_{\mathrm{MgO}} + 3\,\chi_{\mathrm{Fe_2O_3}} + 1\,\chi_{\mathrm{Na_2O}} + 1\,\chi_{\mathrm{K_2O}} \\ &+ 2\,\chi_{\mathrm{TiO_2}})\end{aligned} \tag{A3}$$

$$\chi_{\mathrm{CaO}} \leq \chi_{\mathrm{Al_2O_3}} \text{ and } \chi_{\mathrm{CaO}} + \chi_{\mathrm{MgO}} \geq \chi_{\mathrm{Al_2O_3}}$$

$$\begin{aligned}\Lambda^{\mathrm{C}} = (&1\,\Lambda_{\mathrm{MgO}}\,\Lambda_{\mathrm{CaO}}\left(\chi_{\mathrm{CaO}} + \chi_{\mathrm{MgO}} - \chi_{\mathrm{Al_2O_3}}\right) + 2\,\Lambda_{\mathrm{SiO_2}}\,\chi_{\mathrm{SiO_2}} + 3\,\Lambda_{\mathrm{Al_2O_3}}\,\chi_{\mathrm{Al_2O_3}} + 3\,\Lambda_{\mathrm{Fe_2O_3}}\,\chi_{\mathrm{Fe_2O_3}} + 1\,\Lambda_{\mathrm{Na_2O}}\,\chi_{\mathrm{Na_2O}} \\ &+ 1\,\Lambda_{\mathrm{K_2O}}\,\chi_{\mathrm{K_2O}} + 2\,\Lambda_{\mathrm{TiO_2}}\,\chi_{\mathrm{TiO_2}})/(1\left(\chi_{\mathrm{CaO}} + \chi_{\mathrm{MgO}} - \chi_{\mathrm{Al_2O_3}}\right) + 2\,\chi_{\mathrm{SiO_2}} + 3\,\chi_{\mathrm{Al_2O_3}} + 3\,\chi_{\mathrm{Fe_2O_3}} + \\ &1\,\chi_{\mathrm{Na_2O}} + 1\,\chi_{\mathrm{K_2O}} + 2\,\chi_{\mathrm{TiO_2}})\end{aligned} \tag{A4}$$

The correction for optical basicity will not be required when $\chi_{CaO} + \chi_{MgO} \leq \chi_{Al_2O_3}$ because in this condition, the aluminum oxide will behave as a basic oxide and the Al^{3+} ions will not incorporated into the Si^{4+} chain or rig. In this case, Eq (A2) is applied as is, without correction. The coefficients A_{NPL} and B_{NPL} can be calculated according to the expressions

$$\ln \frac{B_{\mathrm{NPL}}}{1000} = -1.77 + \frac{2.88}{(\Lambda^{\mathrm{C}} \text{or } \Lambda^{\mathrm{NC}})} \tag{A5}$$

$$\ln A_{\mathrm{NPL}} = -232.69(\Lambda^{\mathrm{C}} \text{or } \Lambda^{\mathrm{NC}})^2 + 357.32(\Lambda^{\mathrm{C}} \text{or } \Lambda^{\mathrm{NC}}) - 144.17 \tag{A6}$$

The accuracy of the present method is not reported in the original work [37]. However, by using the data proposed by Duffy and Ingram [38], it is possible to estimate the deviations between the theoretical and the experimental optical basicity values. The data refers to glassy materials and the confidence band is equal to about ± 9 %.

APPENDIX B

In Table B1, the nameplate data for the selected gas turbine are reported. The data are indicative and based on GTPRO® estimates and calculations according to the operating conditions reported in this paper.

List of table captions

Table 1 – Fly-ash material characterization (material composition in terms of weight fraction, ash content refers to dry conditions)

Table 2 – Best and worst gas turbines according to the contaminant

Table A1 – Values of theoretical optical basicity Λ

Table B1 – The nameplate data of the selected heavy-duty gas turbines: pressure ratio (PR), turbine inlet temperature (TIT), air mass flow rate m, net power P and efficiency η

List of figure captions

Journal of Engineering for Gas Turbines and Power. Received July 27, 2018;
Accepted manuscript posted August 23, 2018. doi:10.1115/1.4041249

Table 1 – Fly-ash material characterization (material composition in terms of weight fraction, ash content refers to dry conditions)

	T_{soft} [K]	Ash [%]	Oxides (wt%)							
			Na_2O	K_2O	CaO	MgO	SiO_2	Al_2O_3	TiO_2	Fe_2O_3
Petcoke	1162 [×]	0.7 [+]	4.3	2.5	7.5	2.2	38.3	14.5	0.8	22.9
Straw	1213 [2×]	3.3 [2+]	1.7	23.4	7.8	2.5	48.4	1.8	0.0	5.0
VAT-2	1438 [3×]	6.8 [3+]	0.7	0.4	8.5	2.0	37.0	16.0	2.0	7.9
Pittsburgh	1589 [4×]	6.9 [4+]	0.9	1.2	5.8	1.2	47.9	25.0	1.3	10.9
VAT-1	1773 [5×]	10.0 [5+]	0.4	1.2	2.3	1.1	39.0	26.0	1.3	9.0

[×] Estimated with the model of Yin *et al.* [27]

[+] Average values taken from Phyllis database [20]

[2×] Estimated with the model of Yin *et al.* [27]

[2+] Taken from Phyllis database [20]

[3×] Taken from Trent *et al.* [26]

[3+] Taken from Trent *et al.* [26]

[4×] Taken from Anderson *et al.* [25]

[4+] Taken from Anderson *et al.* [25]

[5×] Taken from Trent *et al.* [26]

[5+] Taken from Trent *et al.* [26]

Journal of Engineering for Gas Turbines and Power. Received July 27, 2018;
Accepted manuscript posted August 23, 2018. doi:10.1115/1.4041249

Table 2 – Best and worst gas turbines according to the contaminant

	Best		Worst	
	Turbine	m_{cont} **[kg/s]**	**Turbine**	m_{cont} **[kg/s]**
petcoke	SIE SGT5-8000H	0.66	KHI GPB30D	1.13
straw	SIE SGT5-8000H	3.27	KHI GPB30D	5.55
VAT-2	SOL Saturn 20-T1600	0.09	GE NovaLT5-1	8.89
Pittsburgh	SOL Saturn 20-T1600	0.02	GE 6111FA	7.74
VAT-1	SOL Saturn 20-T1600 GE 5251M	0.01	MTSB HIT 501G	10.04

Journal of Engineering for Gas Turbines and Power. Received July 27, 2018;
Accepted manuscript posted August 23, 2018. doi:10.1115/1.4041249

Table A1 – Values of theoretical optical basicity Λ

K_2O	Na_2O	CaO	MgO	Al_2O_3	TiO_2	SiO_2	Fe_2O_3
1.40	1.15	1.00	0.78	0.60	0.61	0.48	0.75

Journal of Engineering for Gas Turbines and Power. Received July 27, 2018;
Accepted manuscript posted August 23, 2018. doi:10.1115/1.4041249

Table B1 – The nameplate data of the selected heavy-duty gas turbines: pressure ratio (PR), turbine inlet temperature (TIT), air mass flow rate m, net power P and efficiency η

#	Model	PR	TIT [K]	m [kg/s]	P [kW]	η [%]	#	Model	PR	TIT [K]	m [kg/s]	P [kW]	η [%]
1	ALS GT 5	12.2	1222	15	2726	27.3	51	GE 9351 FA	14.6	1599	648	259670	37.3
2	ALS GT 8	16.5	1423	182	48500	31.7	52	GE 9371FB	18.2	1700	649	291485	38.3
3	ALS GT 8C	15.7	1447	176	52600	34.2	53	GE 9391G	23.2	1706	685	282000	39.5
4	ALS GT 8C 2	17.6	1450	193	57500	34.7	54	MTSB HIT H15	14.3	1546	49	13860	31.3
5	ALS GT 9D	8.9	1233	158	32776	26.6	55	MTSB HIT H25	14.6	1545	88	27010	33.1
6	ALS GT 11N	12.4	1353	311	81600	31.9	56	MTSB HIT 501F	16.0	1673	450	183780	36.9
7	ALS GT 11NM	13.5	1419	315	89600	34.0	57	MTSB HIT 501G	20.0	1772	589	264570	39.4
8	ALS GT 11N2	15.1	1419	375	113700	37.4	58	MTSB HIT 701F	17.0	1673	635	278300	38.7
9	ALS GT 13D2	12.5	1314	400	100500	32.2	59	MTSB HIT 701G	21.0	1700	737	334000	39.5
10	ALS GT 13E	14.1	1367	491	148000	34.6	60	KHI GPB15D	9.6	1274	8	1480	24.0
11	ALS GT 13E2	15.0	1377	514	164300	35.7	61	KHI GPB15	9.4	1228	8	1515	24.4
12	GE PGT 2	12.7	1311	11	2000	24.6	62	KHI GPB17D	10.5	1257	8	13540	26.6
13	GE PGT 5	9.1	1312	25	5223	26.9	63	KHI GPB30D	9.6	1275	16	2920	23.8
14	GE NovaLT5-1	14.8	1498	20	5660	30.6	64	KHI GPB30	9.4	1263	16	2915	23.9
15	GE PGT 10	15.6	1352	47	11700	32.0	65	KHI GPB60D	12.9	1368	22	5398	29.2
16	GE 5251M	8.0	1198	97	18115	25.1	66	KHI GPB60	12.7	1379	22	5533	29.6
17	GE 5251RA	8.2	1230	97	20260	26.7	67	KHI GPB70D	15.9	1378	27	6744	30.6
18	GE 5341N	10.2	1266	117	24750	28.7	68	KHI GPB70	15.9	1449	27	6930	30.8
19	GE 5361	10.3	1270	122	25997	28.4	69	KHI GPB80D	16.0	1383	27	7410	32.9
20	GE 5731 PA	10.0	1237	123	26555	28.9	70	KHI GPB80	15.8	1395	27	7800	33.1
21	GE 6101FA	14.8	1561	204	70905	34.3	71	KHI GPB180D	18.6	1524	59	18045	34.0
22	GE 6111FA	15.5	1600	208	82000	35.8	72	MAN MGT6100	14.0	1367	26	6735	31.8
23	GE 6B-03	12.7	1423	143	44220	33.9	73	MAN 1304-10	10.0	1259	44	9310	28.0
24	GE 6531B	11.7	1378	138	40000	31.7	74	MAN 1304-11	11.0	1272	48	10760	29.8
25	GE 6541B	11.8	1378	138	39615	32.5	75	MAN 1304-12	11.0	1287	48	11520	30.6
26	GE 6551B	11.9	1378	141	39870	32.1	76	SIE SGT-300	13.5	1395	30	7900	30.6
27	GE 6561B	12.2	1387	143	40340	32.4	77	SIE SGT-600	13.6	1392	77	21800	32.8

28	GE 6591C	19.0	1599	117	42950	36.4	78	SIE SGT-800	19.0	1561	129	47000	37.5
29	GE 6F.01	20.0	1586	124	53500	38.6	79	SIE SGT-900	15.3	1421	172	49500	32.9
30	GE 7101	11.8	1356	280	77110	32.7	80	SIE W401	18.6	1625	224	85900	36.6
31	GE 7111EA	12.4	1378	293	84920	32.0	81	SIE W701D	14.2	1389	448	132220	34.2
32	GE 7161EC	14.2	1479	352	118685	35.8	82	SIE W701F	16.0	1625	646	252560	37.5
33	GE 7171EF	12.2	1428	413	126200	34.2	83	SIE SGT-1000F	16.1	1561	188	62300	35.2
34	GE 7191F	13.7	1533	420	151300	35.5	84	SIE SGT6-2000E	11.0	1422	354	108719	33.9
35	GE 7221FA	14.8	1561	422	161650	36.9	85	SIE SGT6-3000E	14.2	1450	376	121700	34.7
36	GE 7191F	13.7	1533	420	151300	35.5	86	SIE SGT6-4000F	16.0	1561	425	153600	36.3
37	GE 7221FA	14.8	1561	422	161650	36.9	87	SIE SGT6-5000F	17.0	1623	496	198200	37.7
38	GE 7231FA	15.4	1583	437	171980	37.3	88	SIE SGT6-6000G	20.1	1670	588	266300	39.3
39	GE 7241FA	15.5	1602	448	174000	36.7	89	SIE SGT6-8000H	19.2	1669	638	303180	39.8
40	GE 7251 FB	18.5	1643	445	186600	37.2	90	SIE SGT5-2000E	11.1	1422	500	157010	34.7
41	GE 7821B	10.0	1284	240	61300	31.7	91	SIE SGT5-3000E	14.0	1534	510	189000	36.2
42	GE 9001H	23.2	1705	685	331000	39.5	92	SIE SGT5-4000F	17.0	1589	642	265540	38.7
43	GE 9151E	12.1	1366	405	113700	32.9	93	SIE SGT5-8000H	19.2	1669	858	417265	40.4
44	GE 9161E	12.2	1378	406	119355	33.8	94	SOL Centaur 50	10.7	1328	19	4600	29.3
45	GE 9171E	12.3	1398	410	124700	34.0	95	SOL Mars 90	16.2	1340	39	9286	31.7
46	GE 9231 EC	14.2	1479	515	172985	35.5	96	SOL Mars 100	16.0	1380	38	10000	32.0
47	GE 9281F	13.7	1533	604	217870	35.5	97	SOL Saturn 20-T1600	6.6	1172	7	1210	24.3
48	GE 9301F	13.7	1533	606	214000	35.2	98	SOL Taurus 60	12.0	1333	22	5200	30.6
49	GE 9311FA	14.6	1561	607	231020	36.8	99	SOL Taurus 65-8400	15.4	1494	21	6290	32.7
50	GE 9331FA	14.6	1578	636	245065	36.8	100	SOL Taurus 70	15.0	1394	27	7250	32.8

Journal of Engineering for Gas Turbines and Power. Received July 27, 2018;
Accepted manuscript posted August 23, 2018. doi:10.1115/1.4041249

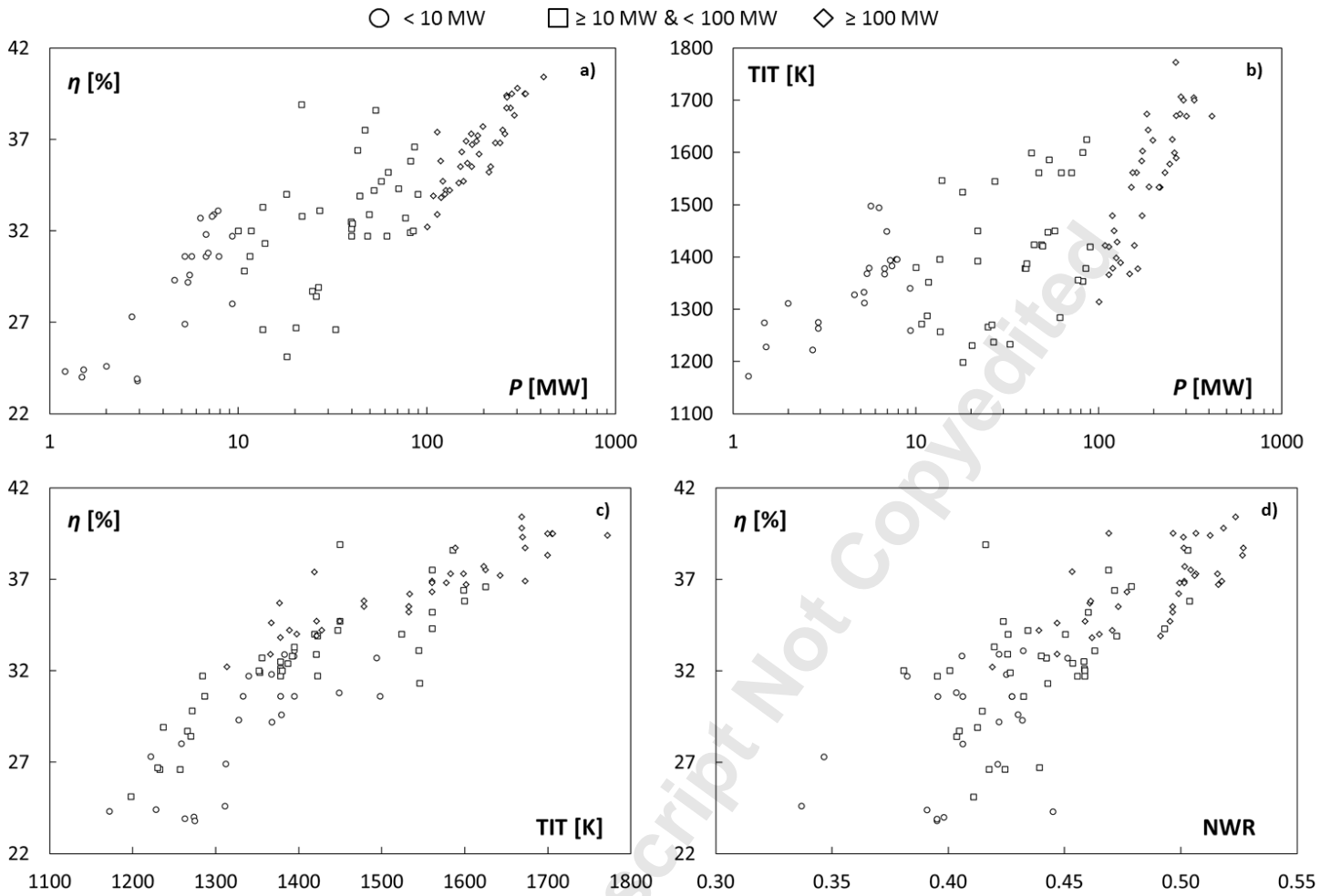

Figure_1_GTP_18-1524.tif

Journal of Engineering for Gas Turbines and Power. Received July 27, 2018;
Accepted manuscript posted August 23, 2018. doi:10.1115/1.4041249

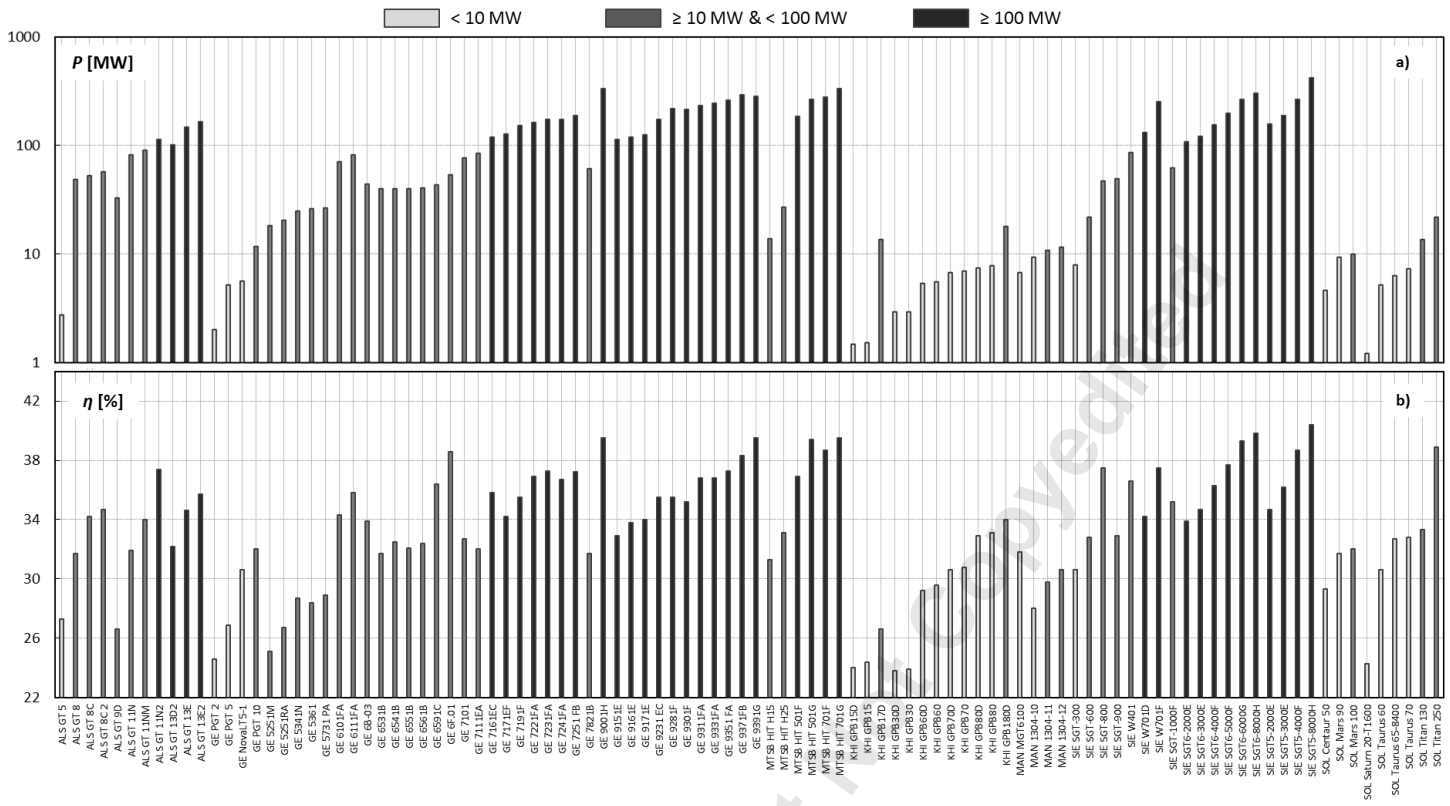

Figure_2_GTP-18-1524.tif

Journal of Engineering for Gas Turbines and Power. Received July 27, 2018;
Accepted manuscript posted August 23, 2018. doi:10.1115/1.4041249

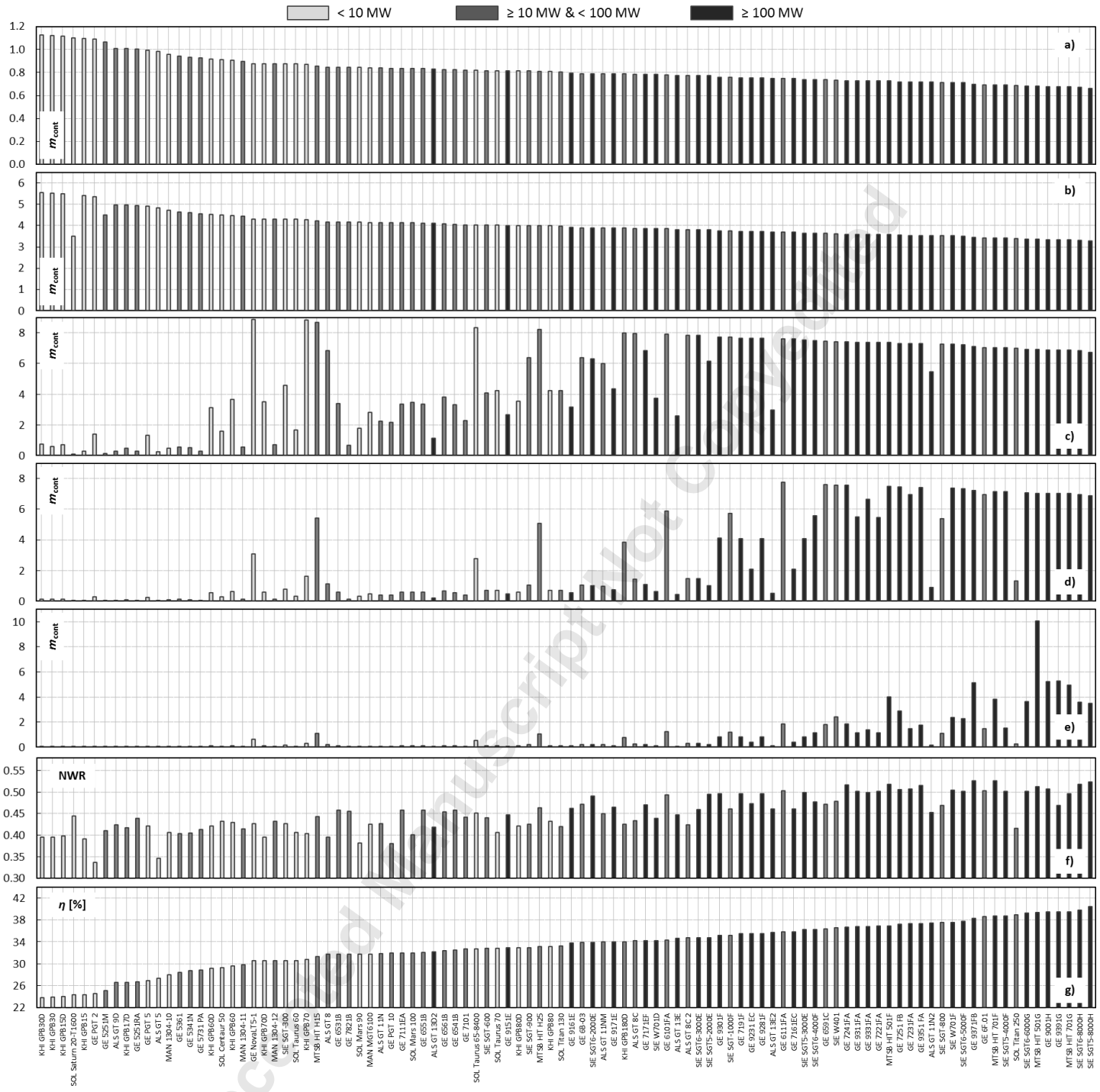

Figure_3_GTP-18-1524.tif

Journal of Engineering for Gas Turbines and Power. Received July 27, 2018;
Accepted manuscript posted August 23, 2018. doi:10.1115/1.4041249

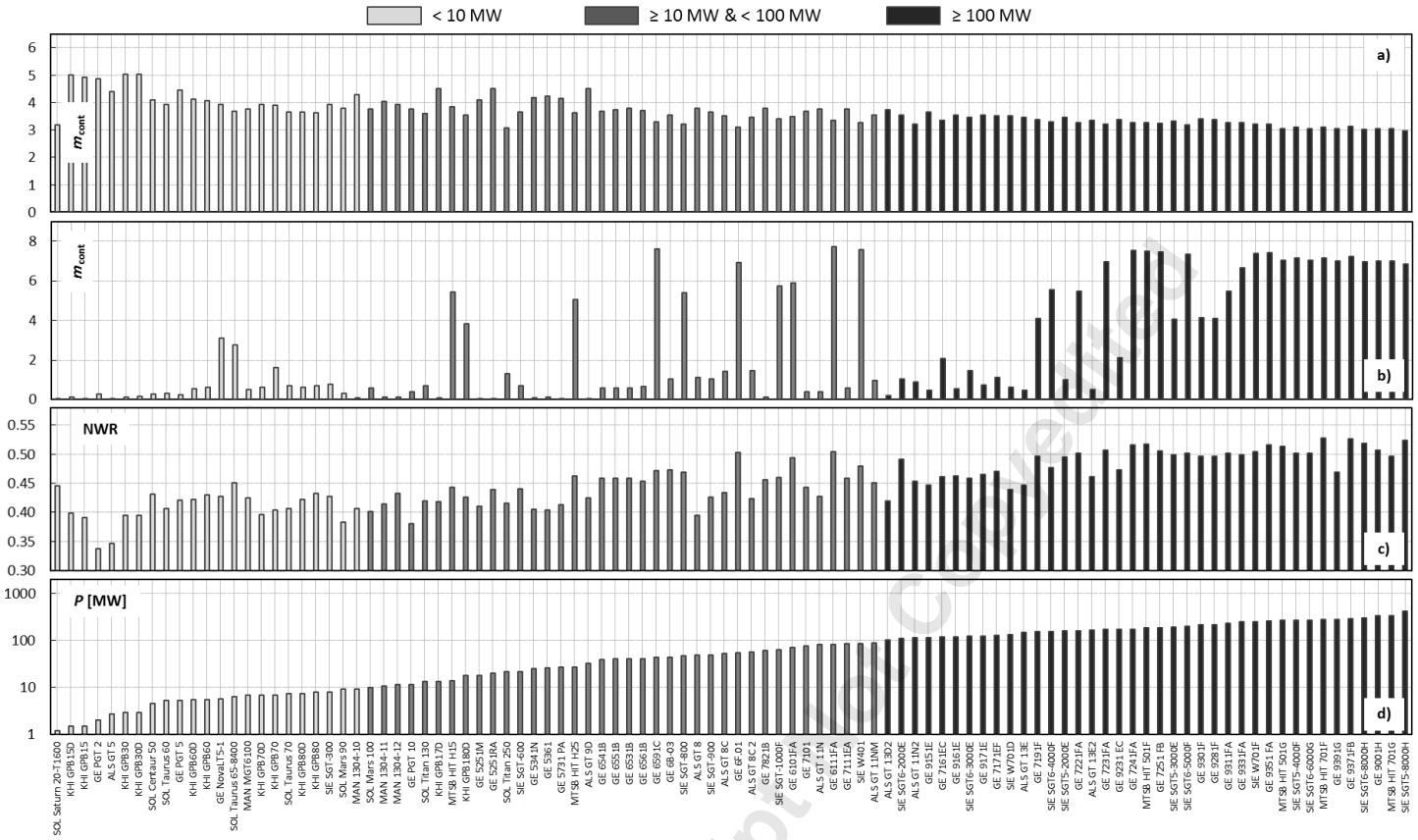

Figure_4_GTP-18-1524.tif

Journal of Engineering for Gas Turbines and Power. Received July 27, 2018;
Accepted manuscript posted August 23, 2018. doi:10.1115/1.4041249

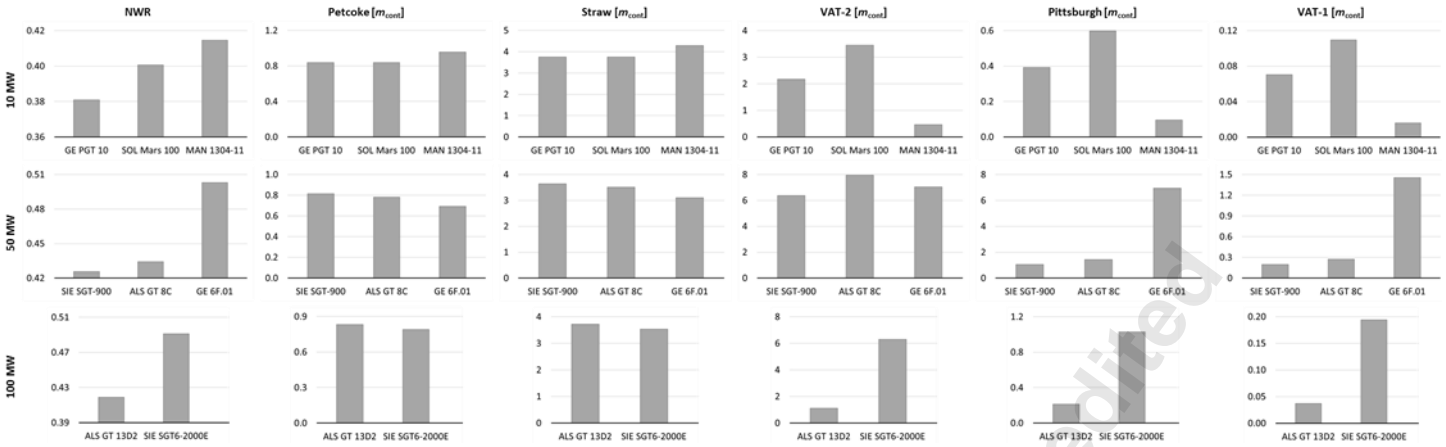

Figure_5_GTP-18-1524.tif

Journal of Engineering for Gas Turbines and Power. Received July 27, 2018;
Accepted manuscript posted August 23, 2018. doi:10.1115/1.4041249

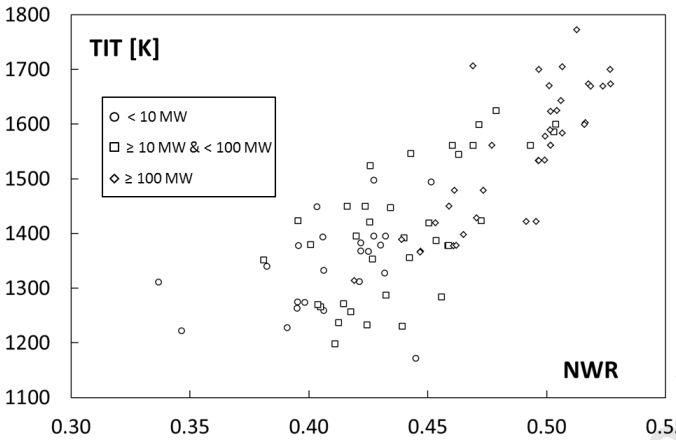

Figure_6_GTP-18-1524.tif

Journal of Engineering for Gas Turbines and Power. Received July 27, 2018;
Accepted manuscript posted August 23, 2018. doi:10.1115/1.4041249

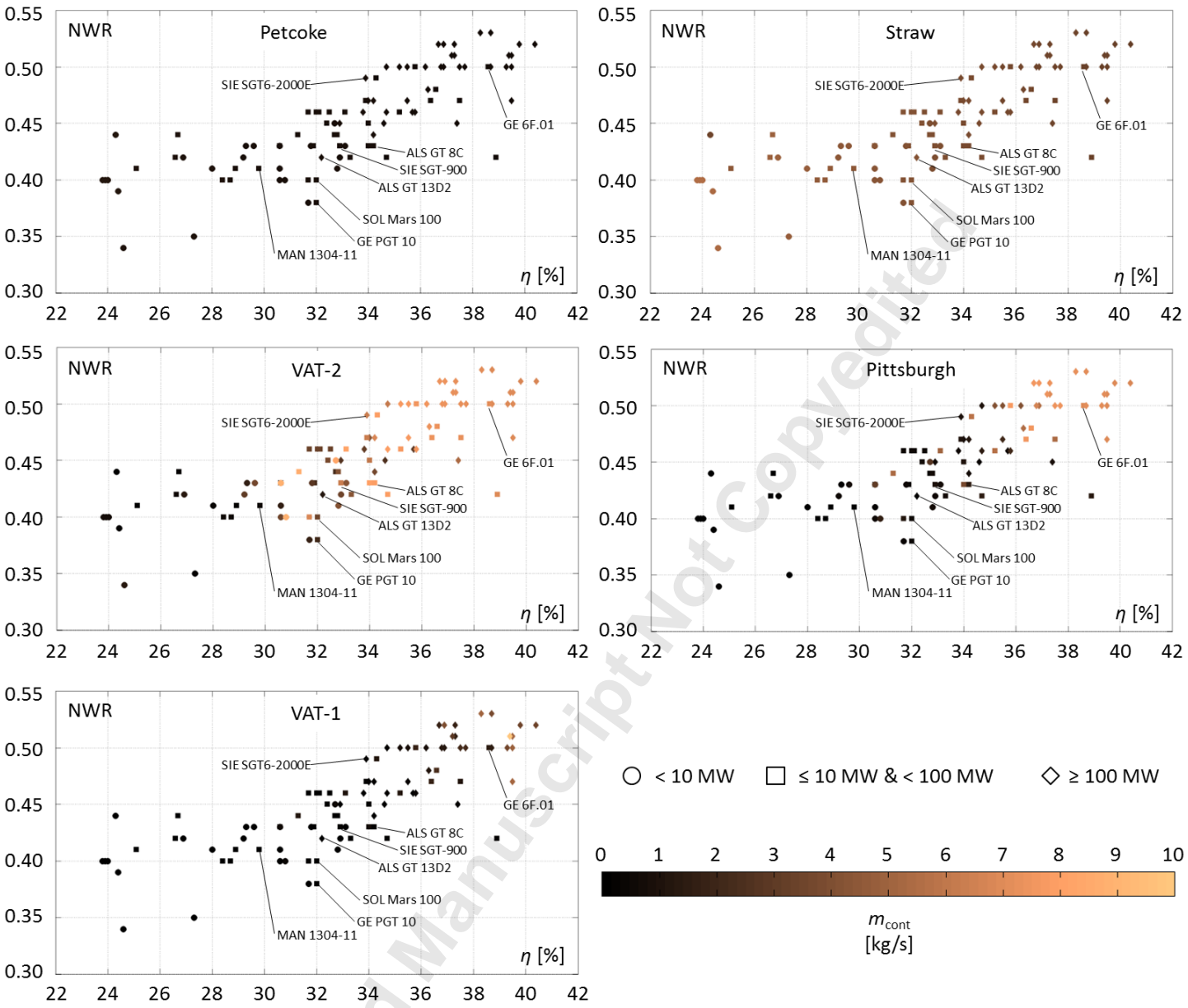

Figure_7_GTP-18-1524.tif